Full Paper

Propellants, Explosives, Pyrotechnics

DOI: 10.1002/prep.201400203

Enhancement of Creep Properties of TATB-Based Polymer-Bonded Explosive Using Styrene Copolymer

Congmei Lin,[a] Jiahui Liu,[a] Zhong Huang,[a] Feiyan Gong,[a] Yubin Li,[a] Liping Pan,[a] Jianhu Zhang,[a] and Shijun Liu*[a]

Abstract: In order to investigate the effects of binder component on the creep properties of polymer-bonded explosive (PBX), three-point bending creep behaviors of 1,3,5-triamino-2,4,6-trinitrobenzene (TATB)-based PBX and its styrene copolymer modified formulation were studied by dynamic mechanical analyzer. The experimental results showed that owing to the addition of reinforcing agent (styrene copolymer) with high glass transition temperature and high mechanical strength, the creep resistance performance of the modified formulation was improved with reduced creep strain and constant creep rate and prolonged creep failure time. A six-element mechanical model was applied to simulate the creep behaviors of TATB-based PBX and its modified formulation. The constitutive equation of creep curves under different conditions were obtained by nonlinear fit. The predicted theoretical results coincided quite well with the experimental data.

Keywords: Applied chemistry · TATB · Polymer bonded explosive · Styrene copolymer · Reinforcing agent · Creep properties

1 Introduction

The creep, which is a time-dependent plastic deformation, takes place at certain temperature and loading stress [1–3]. In recent years, the creep behavior of polymers is of great interest in the academy and industry because of its significant influences on the dimensional stability, long-term durability, and reliability. Consequently, improving the creep resistance of polymer has attracted interest in science and engineering. A common and convenient method is the addition of inorganic nanoparticles [4–6]. It is recognized that with the addition of a low content of inorganic nanoparticles, the creep resistance of polymer could be significantly improved. However, it is also reported that the addition of nanoparticles, such as clay, reduced the creep resistance of polymer due to the decrease of crystal size and degree of crystallinity [7,8]. Besides, it has been demonstrated that the existence of intertube sliding or stick-slip [9] may give rise to an increase in creep rate under low stress [10]. On the other hand, polymer blending has been proved to be an economical, rapid, and versatile method to obtain desirable creep properties in the industrial field [11,12]. It is observed that blending low-creep-speed PS with high-creep-speed PE appears to improve the creep performance of the final composite with reduced creep speed [13].

It is now well accepted that as an insensitive high explosive (IHE) with the advantages of moderately energy output and excellent thermally stability, 1,3,5-triamino-2,4,6-trinitrobenzene (TATB) is extensively applied in military field [14–16]. The polymer-bonded explosives (PBXs) based on TATB, such as LX-17 (92.5% TATB and 7.5% kel-F800 by weight) and PBX-9502 (95% TATB and 5% kel-F800 by weight) have been developed in the last decades [17–19]. The creep relaxation behavior of PBX is a complicated process, which is affected by many factors, for instance, the type of explosive, the percentage and type of binder, the stress level and test temperature [20,21]. High fidelity measurements of time-dependent creep strain in the plastic-bonded explosives LX-17 and PBX-9502 were carried out and it has been revealed that the creep and recovery behavior of PBX is dependent on the percentage of binder, the stress level and test temperature [22]. However, researches on the effects of the type of binder on the creep performance of TATB-based PBX are relatively limited.

PBXs are typically bi-phase composite materials consisting of a mixture of explosive crystals and a polymeric binder. Generally, the explosive component comprises 80–95% of the mass of the composite. Although the ratio of the polymer binder component is limited to a low value, the component and proportion of polymer binder have a marked influence on the properties of PBX, such as thermal decomposition behavior, mechanical properties, failure form, aging resistance, and sensitivity [23–28].

As one kind of the most commonly used binders, fluoropolymer has the advantages of good physical and chemical stability, excellent aging resistance and heat resistance, and

[a] *C. Lin, J. Liu, Z. Huang, F. Gong, Y. Li, L. Pan, J. Zhang, S. Liu*
Institute of Chemical Materials
China Academy of Engineering Physics
Mianyang 621900, Sichuan, P. R. China
**e-mail: lsj99@sohu.com*

great compatibility with other components in composite explosives [29–31]. Compared with general hydrocarbons, the high density of fluoropolymer brings on the enhancement of the density and performance for PBX. On the other hand, styrene copolymer is an engineering thermoplastic with high impact, high transparency and rigidity, good heat stability, and mechanical properties, and it is widely applied in automobile, electrical equipments, mechanical parts, as well as packing containers [32,33]. The blending of fluoropolymer and styrene copolymer provides an effective way to make full use of their respective advantages.

In this work, we focus on the blend of fluoropolymer and styrene copolymer prepared with an internal mixer. The main objective of this study is to investigate the creep relaxation process of TATB-based PBXs with the binders of fluoropolymer and fluoropolymer/styrene copolymer composite by three-point bending creep measurements. The studies on the effects of styrene copolymer on the dynamic mechanical behaviors of composite binder are also conducted.

2 Experimental Section

2.1 Materials

1,3,5-Triamino-2,4,6-trinitrobenzene (TATB) with a purity of 99%, average particle size of 14 μm, a specific surface area of 0.87 $m^2 g^{-1}$, provided by Institute of Chemical Materials, CAEP, China was used. Fluoropolymer with an average molecular weight of 2.74×10^5 $g\,mol^{-1}$and a polydispersity index of 3.37 was supplied by Zhonghao Chenguang Chemical Industry Co., Ltd. China. As a reinforcing agent, styrene copolymer with an average molecular weight of 1.63×10^5 $g\,mol^{-1}$ and a polydispersity index of 1.86 was obtained from Shanghai Gaoqiao Chemical Industry, China. Blend of fluoropolymer and styrene copolymer at composition ratio of 80/20 by weight was prepared with an internal mixer. Before melt blending, fluoropolymer and styrene copolymer were carefully dried in a vacuum oven at 80 °C for 12 h to eliminate the influences of moisture content on the experimental results.

2.2 Sample Preparation

Two TATB-based formulations including 5 mass-% polymer binders were investigated. The original formulation contains only TATB and fluoropolymer. The modified formulation was prepared with the addition of 1 mass-% styrene copolymer as a reinforcing agent. The molding powder of TATB-based polymer bonded explosive (PBX) was prepared with water suspension methods. Ethyl acetate and butyl acetate were selected as the solvent for fluoropolymer and styrene copolymer since TATB was resistant for being dissolved in such system. Afterwards, the molding powder product was pressed in a mould and transformed into explosive sheet with a length of 30 mm, a breadth of 10 mm, and a height of 1–2 mm. The pellet density was about 95% of the theoretical density after compression.

2.3 Dynamic Mechanical Analysis

Dynamic mechanical analysis (DMA) of fluoropolymer, styrene copolymer, and fluoropolymer/styrene copolymer composite was recorded with a DMA 242C apparatus (Netzsch, Germany) in three-point bending creep mode at a frequency of 1 Hz. The specimens for DMA tests with dimensions of 30 mm × 10 mm × 1 mm (length × width × thickness) were molded by an injection molding machine (HAAKE MiniJet). The storage modulus (E′) and loss factor (tan δ) were determined as a function of the temperature, and the heating rate was set for 1 °C min^{-1}.

2.4 Tensile Mechanical Test

Tensile test of the specimens was conducted with a universal testing machine (CMT2000, SANS, China) according to the ASTM D638 standard. The standard dumbbell-shaped specimens (30 mm × 3.1 mm × 3.3 mm, length × width × thickness) for tensile test were molded by a HAAKE MiniJet. The test was performed with a cross head speed of 2 mm min^{-1}. At least five specimens of each binder were tested, and the average values were reported.

2.5 Three-point Bending Creep Test

The three-point bending creep test was conducted with a dynamic mechanical analyzer (DMA 242C, Netzsch, Germany). A Netzsch three-point bending sample holder with a span of 20 mm was employed. The test time was set for 5400 s. If no rupture of sample was observed after 5400 s, the test stopped. If the creep failure of specimens was performed in the examined time, the test finished immediately.

The schematic of the three-point bending creep experiment is presented in Figure 1. The specimen was affected by tensile load and compressive load. The upper surface suffered from compressive load, while the lower surface suffered from tensile load. At a certain center layer, i.e. neutral layer, no tensile stress or compressive stress was loaded on the sample. The bending normal stress presented a linear distribution perpendicular to the neutral layer. The bending normal stress reached maximum on the surface.

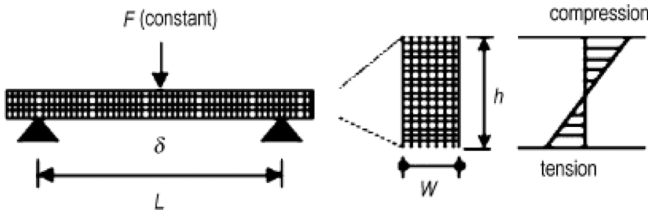

Figure 1. Schematic of three-point bending creep experiment.

The maximum bending normal stress σ_{max} was calculated using the following equation:

$$\sigma_{max} = \frac{3FL}{2wh^2} \quad (1)$$

where F represented the load force, L described the span of sample holder (20 mm), w and h are the sample width and height, respectively.

Table 1. Property parameters of polymer binders.

Sample	Glass transition temperature [°C]	Tensile strength [MPa]	Elongation at break [%]
Fluoropolymer	49.6	14.06	27.73
Styrene copolymer	115.6	64.76	2.477
Composite binder	48.3, 122.4	20.02	10.25

3 Results and Discussion

3.1 The Properties of Polymer Binders

In order to improve the creep resistance of TATB-based PBX, the polymer binder system is enhanced with the addition of reinforcing agent (styrene copolymer). Storage modulus (E′) and loss factor (tan δ) for polymer binders as a function of temperature are shown in Figure 2a and b, respectively. It can be seen that the incorporation of styrene copolymer results in an increase of the storage modulus in the whole temperature range, compared to that of fluoropolymer. On increasing the temperature of polymer, a transition from a glassy state to a rubbery elastic state could be observed. The transition temperature is termed as the glass transition temperature of the polymer, T_g, which has direct relation with the polymer molecular structure. As demonstrated in Figure 2, the T_g of the reinforcing agent (styrene copolymer) are much higher than that of the original binder (fluoropolymer). The main molecular chain of fluoropolymer composes of saturated single bond; therefore, molecular chain could internally rotate surrounding the single bond, leading to a low T_g. However, due to the fact that the main molecular chain of styrene copolymer contains aromatic heterocyclic such as phenyl, the proportion of single bond which could internally rotate is small, and chain stiffness is high. Consequently, the T_g of styrene copolymer is higher than that of fluoropolymer. Based on the original formulation, the modified formulation makes use of the blend of fluoropolymer and styrene copolymer at composition ratio of 80/20 by weight as composite binder with the constant binder total content. The composite binder exists two glass transition temperatures, corresponding to the T_g of fluoropolymer and styrene copolymer, respectively.

The tensile properties of the polymer binders at room temperature were also determined. Table 1 lists the characteristics of the polymer binders, including glass transition temperature T_g, tensile strength, and elongation at break. Compared with the original binder (fluoropolymer), the tensile strength of composite binder increases by 42.4%. The results display that styrene copolymer is an effective reinforcing agent for fluoropolymer binder.

3.2 Three-point Bending Creep Strain Curves of TATB-based PBXs

Figure 3 displays the traces of the creep strain as a function of time for TATB-based PBXs under different maximum bending normal stresses at 60 °C. In terms of the creep time, the creep process could be divided into three characteristic stages. In the primary stage, namely, decelerated creep stage, the creep strain rate, i.e. $\Delta\varepsilon/\Delta t$, is found to diminish with increasing creep time. In the secondary stage, namely, steady creep stage, the creep strain rate keeps constant. In the last stage, namely, accelerated creep stage, the creep strain rate increases with creep time.

As an example, the relationship of the creep time on the creep strain in the steady creep stage of the original formulation at 60 °C/4 MPa is plotted in Figure 4. It is obvious that the creep strain varies linearly with the creep time. The

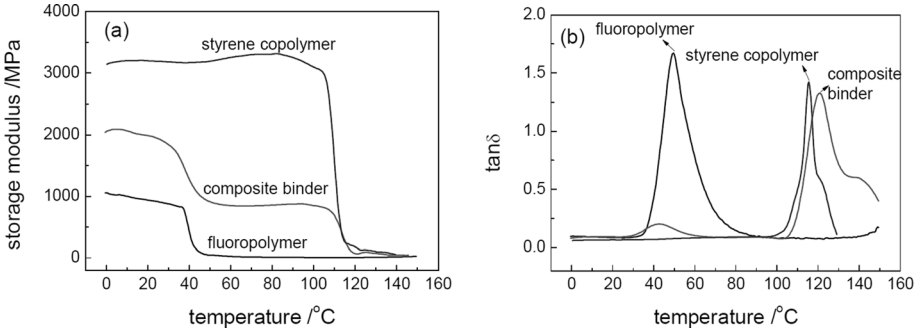

Figure 2. Plot of storage modulus (E′) and loss factor (tan δ) vs. temperature for composite binders: (a) storage modulus (E′), (b) loss factor (tan δ).

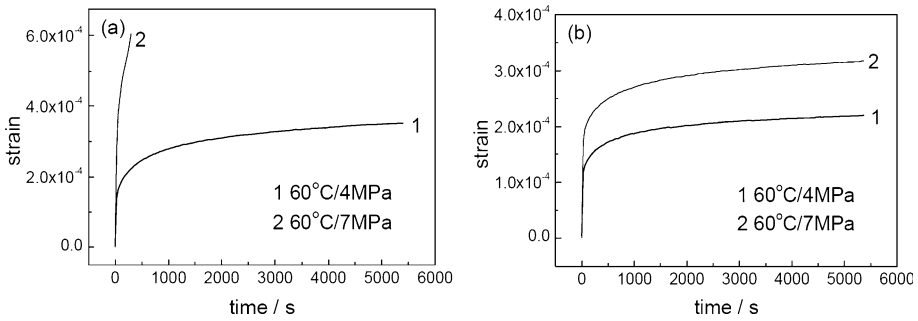

Figure 3. Three-point bending creep strain curves of TATB-based PBXs under different maximum bending normal stresses at 60 °C: (a) the original formulation, (b) the modified formulation.

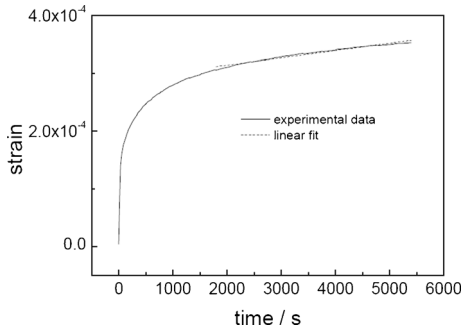

Figure 4. Linear fit of the creep strain curves during steady state of the original formulation at 60 °C/4 MPa.

steady creep rate is the coefficient of creep strain to creep time which are acquired from the slope of the fitting lines in Figure 4. For instance, the steady creep rate of the original formulation at 60 °C/4 MPa is 1.252×10^{-8} s^{-1}. The creep performance parameters of TATB-based PBXs, including constant creep strain rate, creep failure strain and creep failure time are summarized in Table 2.

As can be seen in Figure 3 and Table 2, with the addition of the reinforcing agent (styrene copolymer), a distinct increase is observed in the three-point bending creep resistance of the modified formulation, compared with the original formulation. At 60 °C/4 MPa, it is visibly apparent that the creep strain at $t = 5400$ s and the steady creep rate of the modified formulation decreases by 37.7 % and 58.6 %, respectively. Furthermore, at 60 °C/7 MPa, with regard to the original formulation, the creep strain increases rapidly with creep time, afterwards, creep failure of the sample is occurred at 300 s. Under the same condition, the modified formulation displays a long-term creep process and no creep rupture time could be obtained, suggesting that the creep behavior is improved by the presence of styrene copolymer.

The finding that the three-point bending creep resistance of the modified formulation is higher than that of the original formulation could be interpreted in terms of the motion of chain segment and mechanical strength. The experimental temperature, i.e. 60 °C, is higher than the T_g of the original binder (fluoropolymer). Fluoropolymer is in the rubbery elastic state and its chain segment can freely move and is prone to flow and deform. However, the T_g of the reinforcing agent (styrene copolymer) is much higher than the experimental temperature. Hereby, the reinforcing agent (styrene copolymer) is in the glassy state. The motion of molecular main chain and chain segment is freezed, causing a long relaxation time of the motion of chain segment and a high intermolecular inner frictional resistance. Therefore, the deformation of styrene copolymer decreases. On the other hand, this result could be also explained by the fact that the mechanical strength of fluoropolymer/styrene copolymer blend is higher than that of the original binder (fluoropolymer), as mentioned above.

Creep is a relaxation process, which relies on the existence of the external force. As illuminated in Figure 3 and Table 2, it is clear that the creep resistance depends significantly on the maximum bending normal stress (σ_{max}). At 60 °C/4 MPa, the original formulation presents a long-term creep process, while at 60 °C/7 MPa, the creep rupture time is shortened to 300 s. For the modified formulation, with σ_{max} increased from 4 MPa to 7 MPa at 60 °C, the creep strain and constant creep strain rate enlarges, suggesting that the creep resistance is depressed obviously. The results

Table 2. Creep performance parameters of TATB-based PBXs under different loading stresses at 60 °C.

Sample	Experimental conditions	Constant creep strain rate [s^{-1}]	Creep rupture strain	Creep rupture time [s]
Original formulation	60 °C/4 MPa	1.252×10^{-8}	$>3.526\times10^{-4}$	>5400
	60 °C/7 MPa	–	6.052×10^{-4}	300
Modified formulation	60 °C/4 MPa	5.178×10^{-9}	$>2.195\times10^{-4}$	>5400
	60 °C/7 MPa	7.695×10^{-9}	$>3.176\times10^{-4}$	>5400

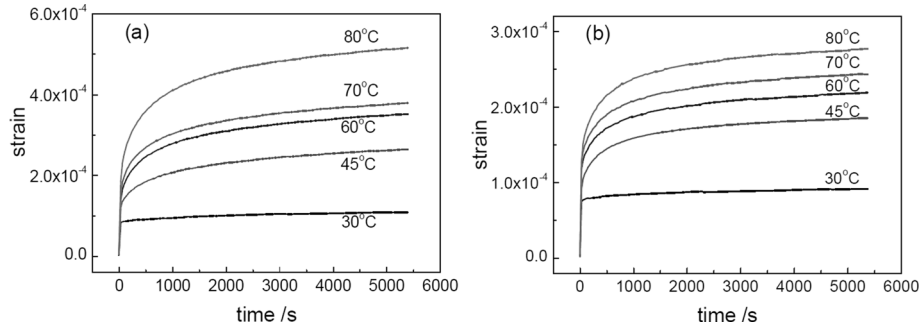

Figure 5. Three-point bending creep strain curves of TATB-based PBXs at different temperatures under 4 MPa: (a) the original formulation, (b) the modified formulation.

Table 3. Creep performance parameters of TATB-based PBXs at different temperatures under 4 MPa.

Sample	Experimental conditions	Constant creep strain rate [s^{-1}]	Creep strain at 5400 s
Original formulation	30 °C/4 MPa	2.390×10^{-9}	1.091×10^{-4}
	45 °C/4 MPa	1.017×10^{-8}	2.647×10^{-4}
	60 °C/4 MPa	1.252×10^{-8}	3.526×10^{-4}
	70 °C/4 MPa	1.294×10^{-8}	3.803×10^{-4}
	80 °C/4 MPa	1.705×10^{-8}	5.161×10^{-4}
Modified formulation	30 °C/4 MPa	1.390×10^{-9}	9.166×10^{-5}
	45 °C/4 MPa	4.291×10^{-9}	1.856×10^{-4}
	60 °C/4 MPa	5.178×10^{-9}	2.195×10^{-4}
	70 °C/4 MPa	5.782×10^{-9}	2.433×10^{-4}
	80 °C/4 MPa	6.234×10^{-9}	2.771×10^{-4}

indicate that the dimensional stability and long-term load capacity reduce with increasing loading stress. The results that creep resistance is associated with the loading stress could be explained by the role of loading stress on the deformation of the molecular chain. The high loading stress brings on a decrease of viscosity, so the motion of molecular chain becomes easier.

Creep is a typical viscoelastic phenomenon of PBX, which is intimately correlated to temperature. The effects of temperature on the creep behavior are also explored, as depicted in Figure 5 and Table 3. In the experimental test, 4 MPa is carefully selected as the applied stress within the elastic range. The experimental results reveal a strong dependence of the creep resistance on the temperature. It is evident that with temperature increased from 30 °C to 80 °C under 4 MPa, the creep strain of the original formulation at 5400 s increases from 1.091×10^{-4} to 5.161×10^{-4}, the constant creep strain rate enlarges from $2.390\times10^{-9}\ s^{-1}$ to $1.705\times10^{-8}\ s^{-1}$, revealing that the creep resistance reduces. Similar behavior is displayed by the modified formulation. The fact that the creep resistance decreases with increasing temperature is attributed to an enhancement in molecular thermodynamic movement. As temperature increases, the energy of thermodynamic motion enhanced. On the other hand, the volume of binder expands with the temperature increment, causing an increase in the intermolecular free space. Two actions result in the aggravation of molecular thermodynamic movement. The binder becomes soft, inducing interfacial debonding of binder and TATB particles. Consequently, the creep resistance of TATB-based PBXs reduces with temperature.

3.3 Constitutive Equation of Creep Curve

In an attempt to deeply understand the creep mechanical relaxation behavior, many researchers propose that the creep process could be simulated by the combination of ideal spring and ideal dashpot in different forms, such as Maxwell model, Voigt (or Kelvin) model and Burger four-element mechanical model [34–36]. Among them, as a combination of Maxwell and Voigt elements, Burger four-element mechanical model is one of the most used models to give the relationship between the morphology of the composites and their creep behavior [6]. However, Burger four-element mechanical model only gives the exponential response with single relaxation time. PBX is a kind of particle highly-filled composite material based on polymer. On account of the multiplicity of structure units and complexity of molecular motion, not only one relaxation time exists in the creep process. Therefore, multiple element mechanical models should be adopted to simulate the creep process. In this work, a six-element mechanical model is employed to describe the creep process, as shown in Figure 6.

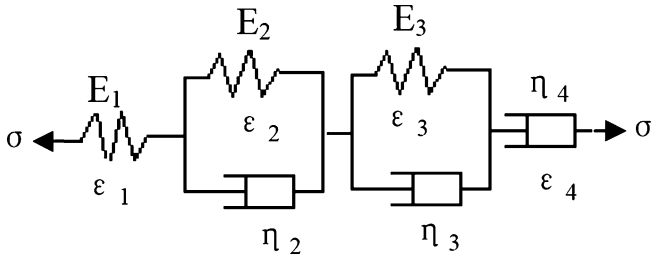

Figure 6. Schematic drawing of six-element mechanical model.

The six-element mechanical model can be regarded as a series connection structure of a Maxwell model and two Voigt models. During the creep process, $\sigma=\sigma_0$, consequently, the total strain of polymer composite material PBX could be determined by:

$$\varepsilon(t)=\varepsilon_1+\varepsilon_2+\varepsilon_3+\varepsilon_4=\frac{\sigma_0}{E_1}+\frac{\sigma_0}{E_2}\left(1-e^{-t/\tau_2}\right)+\frac{\sigma_0}{E_3}\left(1-e^{-t/\tau_3}\right)+\frac{\sigma_0}{\eta_4}t \quad (2)$$

where $\varepsilon(t)$ denotes a function of creep strain ε with creep time t, ε_1 is the instantaneous elastic deformation, ε_2 and ε_3 are the high elastic deformation, ε_4 is the viscous flow deformation, σ_0 is the initial stress, E_1 is the elastic modulus of instantaneous elastic deformation, E_2 and E_3 are the elastic modulus of high elastic deformation, τ_2 and τ_3 are the relaxation time, η_4 is the bulk viscosity, respectively. Among them, $\tau_2=\eta_2/E_2$ and $\tau_3=\eta_3/E_3$ represent the time taken to produce 63.2% or $(1-e^{-1})$ of the total deformation in Voigt units, where η_2 and η_3 are related to the viscosity of Voigt units.

Equation (2) divides by σ_0:

$$\frac{\varepsilon(t)}{\sigma_0}=\frac{1}{E_1}+\frac{1}{E_2}\left(1-e^{-t/\tau_2}\right)+\frac{1}{E_3}\left(1-e^{-t/\tau_3}\right)+\frac{1}{\eta_4}t \quad (3)$$

During the creep process, the loading stress is regarded as a constant value, and therefore, the creep process can be also characterized with the creep compliance D. The creep compliance can be calculated as:

$$D(t)=\frac{\varepsilon(t)}{\sigma_0} \quad (4)$$

Equation (3) is transferred to the creep compliance equation:

$$D(t)=\frac{1}{E_1}+\frac{1}{E_2}\left(1-e^{-t/\tau_2}\right)+\frac{1}{E_3}\left(1-e^{-t/\tau_3}\right)+\frac{1}{\eta_4}t \quad (5)$$

Equation (5) is the constitutive equation of creep compliance curve.

Figure 7 shows three-point bending creep compliance curves of TATB-based PBXs at different temperatures under 4 MPa. As an example, the experimental curve of creep compliance for the original formulation at 30 °C/4 MPa is fitted by means of six-element mechanical model using Origin data analysis software, as given in Figure 8. It can be

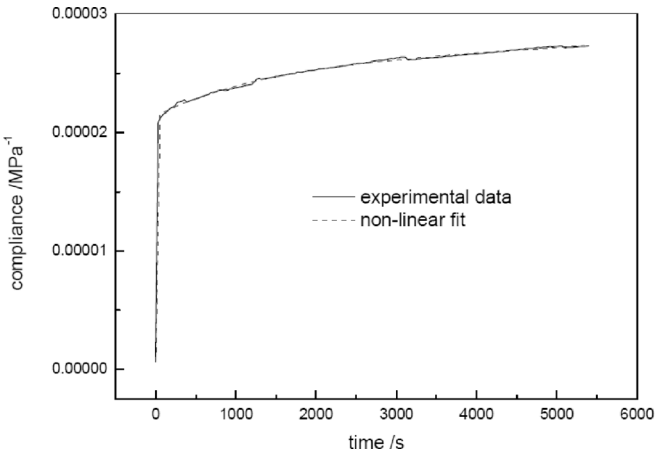

Figure 8. Three-point bending creep compliance curve and non-linear fitting curve of the original formulation at 30 °C/4 MPa.

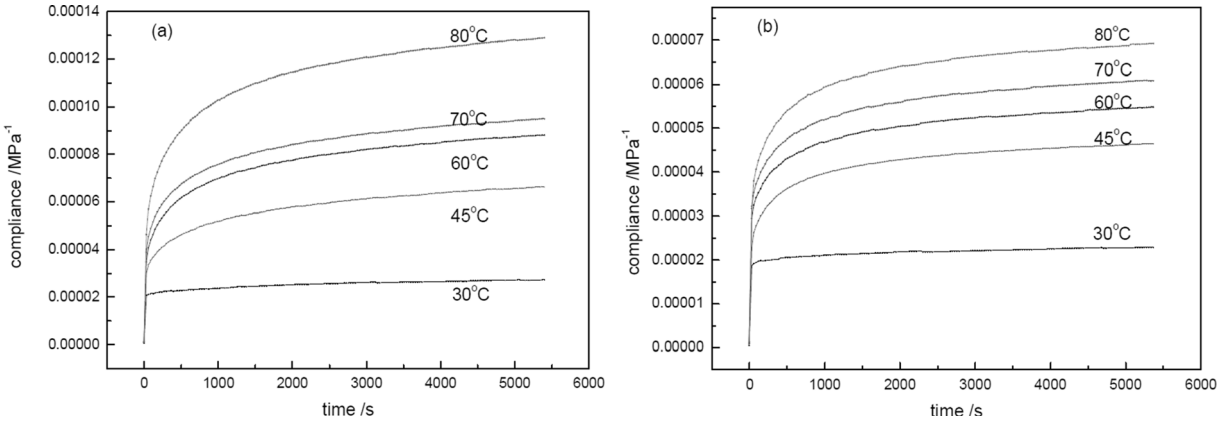

Figure 7. Three-point bending creep compliance curves of TATB-based PBXs at different temperatures under 4 MPa: (a) the original formulation, (b) the modified formulation.

Table 4. Fitting parameters of the six-element model under different conditions.

Test condition	E_1 [MPa]	E_2 [MPa]	τ_2 [s]	η_2 [MPa s]	E_3 [MPa]	τ_3 [s]	η_3 [MPa s]	η_4 [MPa s]	R^2
Sample: Original formulation									
30 °C/4 MPa	1.605×10^6	2.473×10^5	1317.32	3.257×10^8	4.818×10^4	8.82	4.249×10^5	2.754×10^9	0.99848
45 °C/4 MPa	1.078×10^6	4.878×10^4	682.79	3.331×10^7	3.022×10^4	17.03	5.146×10^5	4.398×10^8	0.99889
60 °C/4 MPa	8.130×10^5	3.198×10^4	616.17	1.971×10^7	2.445×10^4	21.62	5.286×10^5	3.493×10^8	0.99865
70 °C/4 MPa	6.879×10^5	3.083×10^4	618.48	1.907×10^7	2.182×10^4	21.69	4.733×10^5	3.376×10^8	0.99857
80 °C/4 MPa	5.272×10^5	2.039×10^4	633.48	1.292×10^7	1.710×10^4	26.35	4.506×10^5	2.638×10^8	0.99883
Sample: Modified formulation									
30 °C/4 MPa	2.089×10^6	5.280×10^5	590.12	3.116×10^8	5.329×10^4	8.71	4.641×10^5	2.926×10^9	0.99859
45 °C/4 MPa	1.348×10^6	6.808×10^4	548.84	3.737×10^7	3.874×10^4	18.23	7.062×10^5	9.814×10^8	0.99846
60 °C/4 MPa	8.847×10^5	6.291×10^4	562.18	3.537×10^7	3.170×10^4	15.28	4.844×10^5	8.203×10^8	0.99834
70 °C/4 MPa	7.522×10^5	5.438×10^4	561.79	3.055×10^7	2.917×10^4	16.19	4.723×10^5	7.336×10^8	0.99848
80 °C/4 MPa	5.594×10^5	4.383×10^4	540.87	2.371×10^7	2.698×10^4	20.84	5.622×10^5	6.734×10^8	0.99829

seen that the modeling curve shows a satisfactory agreement with the experimental data. The non-linear curve fit function was adopted and non-linear fitting parameters including the elastic modulus E_1, E_2, E_3, the relaxation time τ_2, τ_3, the viscosity of Voigt units η_2, η_3, and the bulk viscosity η_4 of TATB-based PBXs were defined, as listed in Table 4. As shown in Table 4, square values of fitting correlation coefficient R^2 are all above 0.99829, suggesting that the six-element mechanical model can effectively describe the three-point bending creep behaviors with high precision.

As can be seen from the fitting parameters in Table 4, the elastic modulus of instantaneous elastic deformation E_1 gradually decreases with increasing temperature of TATB-based PBXs at 4 MPa. E_1 is related to the Maxwell spring, establishing instantaneous creep strain that would be recovered after stress elimination. As analyzed above, the enhancement in the energy of molecular thermodynamic motion and the volume expansion of binder result in the aggravation of molecular thermodynamic movement. Macroscopically, the rigidity of material decreases, leading to a decrease of the elastic modulus. The elastic modulus of high elastic deformation E_2 and E_3 of TATB-based PBXs are sensitive to temperature. It shows that the bulk viscosity η_4 is much higher than the viscosity of Voigt units η_2 and η_3. The bulk viscosity η_4, which reflects the irrecoverable creep strain manifests a distinct dependence on temperature. It can be clear observed that η_4 decreases with increasing temperature, indicating that lower flow is occurred and the permanent deformation reduces. The relative slide of molecular chain of binder could be easier as temperature increases. It can also be seen that all of these parameters display a decreasing trend with the addition of the reinforcing agent (styrene copolymer). In view of the results, it seems reasonable to believe the elastic modulus E_1, E_2, E_3 and bulk viscosity η_4 could be promising for the evaluation of the creep resistance of TATB-based PBXs.

4 Conclusions

Styrene copolymer was used as a reinforcing agent in the 1,3,5-triamino-2,4,6-trinitrobenzene (TATB)-based polymer-bonded explosive (PBX) to examine the influences of styrene copolymer, temperature and loading stress on the creep properties of TATB-based PBXs. The experimental results indicated that: (1) the creep resistance was affected evidently by the addition of styrene copolymer. It was found that a decrease of the creep strain and constant creep strain rate of styrene copolymer modified TATB-based PBX was attributed to the enhancement of the glass transition temperature and the mechanical strength of polymer binder; (2) the creep resistance was also sensitive to temperature and loading stress. Owing to an increase in intermolecular free volume fraction and an aggravation of molecular thermodynamic movement, TATB-based PBXs with or without styrene copolymer displayed a very pronounced decrease in the creep resistance with increasing temperature and loading stress. (3) Six-element mechanical model can effectively describe the three-point bending creep behaviors of TATB-based PBXs with high precision. The experimental results indicated that the elastic modulus of instantaneous elastic deformation E_1, the elastic modulus of high elastic deformation E_2 and E_3, and the bulk viscosity η_4 were sensitive and promising for the evaluation of the creep resistance of TATB-based PBXs. Therefore, the elastic modulus E_1, E_2, E_3 and the bulk viscosity η_4 may be taken as characteristic creep relaxation parameters for TATB-based PBXs.

References

[1] B. B. Tian, Z. H. Chen, A. Q. Jiang, X. L. Zhao, B. L. Liu, J. L. Wang, L. Han, Sh. Sun, J. L. Sun, X. J. Meng, J. H. Chu, The Creep Process of the Domain Switching in Poly(vinylidene fluoride-trifluoroethylene) Ferroelectric Thin Films, *Appl. Phys. Lett.* **2013**, *103*, 042909.

[2] Y. C. Hsueh, L. H. Lai, T. F. Tseng, J. Y. Wu, S. T. Shiue, Microbending Losses in Double-Coated Optical Fibers Caused by Axial

Strain-Induced Creep Deformation of Polymeric Coatings, *J. Appl. Phys.* **2010**, *108*, 053519.
[3] L. C. Tang, X. Wang, L. X. Gong, K. Peng, L. Zhao, Q. Chen, L. B. Wu, J. X. Jiang, G. Q. Lai, Creep and Recovery of Polystyrene Composites Filled with Graphene Additives, *Composites Sci. Technol.* **2014**, *91*, 63 – 70.
[4] H. S. Xia, M. Song, Z. Y. Zhang, M. Richardson, Microphase Separation, Stress Relaxation, and Creep Behavior of Polyurethane Nanocomposites, *J. Appl. Polym. Sci.* **2007**, *103*, 2992 – 3002.
[5] H. Münstedt, T. Köppl, C. Triebel, Viscous and Elastic Properties of Poly(methylmethacrylate) Melts Filled with Silica Nanoparticles, *Polymer* **2010**, *51*, 185 – 191.
[6] Y. Jia, K. Peng, X. L. Gong, Creep and Recovery of Polypropylene/Carbon Nanotube Composites, *Int. J. Plasticity* **2011**, *27*, 1239 – 1251.
[7] L. Shen, I. Y. Phang, L. Chen, T. X. Liu; K. Y. Zeng. Nanoindentation and Morphological Studies on Nylon 66 Nanocomposites. I. Effect of Clay Loading, *Polymer* **2004**, *45*, 3341–3349.
[8] B. D. Beake, S. Chen, J. B. Hull, F. Gao, Nanoindentation Behavior of Clay/poly(ethyleneoxide) Nanocomposites, *J. Nanosci. Nanotechnol.* **2002**, *2*, 73 – 79.
[9] J. Suhr, N. Koratkar, P. Keblinski, P. Ajayan, Viscoelasticity in Carbon Nanotube Composites, *Nat. Mater.* **2005**, *4*, 134 – 137.
[10] J. L. Yang, Z. Zhang, K. Friedrich, A. K. Schlarb. Creep Resistant Polymer Nanocomposites Reinforced with Multiwalled Carbon Nanotubes, *Macromol. Rapid Commun.* **2007**, *28*, 955 – 961.
[11] R. D. Maksimov, T. Ivanova, J. Zicans, Creep of Poly(Vinylchloride)/Chlorinated Polyethylene Blends, *Mechanics Composite Mater.* **2002**, *38*, 291 – 298.
[12] S. Dadbin, M. Frounchi, M. Sabet, Studies on the Properties and Structure of Electron-Beam Crosslinked Low-Density Polyethylene/poly[ethylene-co-(vinyl Acetate)] Blends, *Polym. Internat.* **2005**, *54*, 686–691.
[13] B. Xu, J. Simonsen, W. E. Rochefort, Mechanical Properties and Creep Resistance in Polystyrene/polyethylene Blends, *J. Appl. Polym. Sci.* **2000**, *76*, 1100 – 1108.
[14] J. T. Mang, R. P. Hjelm, Fractal Networks of Inter-Granular Voids in Pressed TATB, *Propellants Explos. Pyrotech.* **2013**, *38*, 831 – 840.
[15] Z. J. Yang, J. S. Li, B. Huang, S. J. Liu, Z. Huang, F. D. Nie, Preparation and Properties Study of Core-Shell CL-20/TATB Composites, *Propellants Explos. Pyrotech.* **2014**, *39*, 51–58.
[16] C. Zhang, Y. Ma, D. Jiang, Charge Transfer in TATB and HMX Under Extreme Conditions, *J. Mol. Modeling* **2012**, *18*, 4831 – 4841.
[17] R. L. Gustavsen, R. J. Gehr, S. M. Bucholtz, R. R. Alcon, B. D. Bartram, Shock Initiation of the Tri-amino-tri-nitro-benzene based Explosive PBX 9502 Cooled to −55 °C, *J. Appl. Phys.* **2012**, 112, 074909.
[18] C. Souers, P. Lewis, M. Hoffman, B. Cunningham, Thermal Expansion of LX-17, PBX 9502, and Ultrafine TATB, *Propellants Explos. Pyrotech.* **2011**, *36*, 335–340.
[19] W. Small IV, E. A. Glascoe, G. E. Overturf, Measurement of Moisture Outgassing of the Plastic-Bonded TATB Explosive LX-17, *Thermochim. Acta* **2012**, *545*, 90–95.
[20] B. J. Cunningham, F. J. Gagliardi, Effects of Temperature Change During a PBX 9502 Constant Stress Compressive Creep Test, LLNL Internal Report, Livermore, CA, USA, February **2008**.
[21] B. J. Cunningham, F. J. Gagliardi, C. Hrousis, I. Darnell, *Predicting Creep Compression Failure in LX-17 and PBX 9502*, LLNL Internal Report, Livermore, CA, USA, August **2006**.
[22] F. J. Gagliardi, B. J. Cunningham. *Creep Testing Plastic-Bonded Explosives in Uni-Axial Compression*, Report LLNL-CONF-402307, Livermore, CA, USA, **2008**.
[23] S. F. Trevino, D. A. Wiegand, Mechanically Induced Damage in Composite Plastic-Bonded Explosives: A Small Angle Neutron and X-ray Study, *J. Energ. Mater.* **2008**, *26*, 79–80.
[24] C. M. Tarver, J. G. Koerner, Effects of Endothermic Binders on Times to Explosion of HMX- and TATB-Based Plastic-Bonded Explosives, *J. Energ. Mater.* **2008**, *26*, 1–28.
[25] D. M. Hoffman, Dynamic Mechanical Signatures of Aged LX-17-1 Plastic-Bonded Explosive, *J. Energ. Mater.* **2001**, *19*, 163–193.
[26] H. F. Rizzo, J. R. Humphrey, J. R. Kolb. Growth of 1,3,5-Triamino-2,4,6-trinitrobenzene (TATB). II Control of Growth by Use of High T_g Polymeric Binders, UCRL-81189, **1980**.
[27] J. J. Xiao, X. F. Ma, W. Zhu, Y. Huang, H. Xiao, H. H., J. Li, Molecular Dynamics Simulations of Polymer-Bonded Explosives (PBXs): Modeling, Mechanical Properties and their Dependence on Temperatures and Concentrations of Binders, *Propellants Explos. Pyrotech.* **2007**, *32*, 355–359.
[28] X. F. Ma, J. J. Xiao, H. Huang, X. H. Ju, J. S. Li, H. M. Xiao, Simulative Calculation of Mechanical Property, Binding Energy and Detonation Property of TATB/fluorine-polymer PBX, *Chin. J. Chem.* **2006**, *24*, 473 – 477.
[29] D. M. Hoffman, Dynamic Mechanical Signatures of Viton A and Plastic-Bonded Explosives Based on this Polymer, *Polym. Eng. Sci.* **2003**, *43*, 139 – 156.
[30] L. L. Stevens, D. M. Dattelbaum, M. Ahart, R. J. Hemley, High-Pressure Elastic Properties of a Fluorinated Copolymer: Poly(-chlorotrifluoroethylene-co-vinylidene Fluoride) (Kel-F 800), *J. Appl. Phys.* **2012**, *112*, 023523.
[31] Q. L. Yan, S. Zeman, A. Elbeih, Thermal Behavior and Decomposition Kinetics of Viton A-Bonded Explosives Containing Attractive Cyclic Nitramines, *Thermochim. Acta* **2013**, *562*, 56 – 64.
[32] X. Meng, X. Liu, Z. Li, Q. Zhou, Positron Annihilation Lifetime Spectroscopy for Miscibility Investigations of Styrene-Butadiene-Styrene Copolymer/Polystyrene Blends, *Polym. Eng. Sci.* **2014**, *54*, 785 – 793.
[33] U. A. Handge, C. Sailer, H. Steininger, M. Weber, S. Scholtyssek, V. Seydewitz, G. H. Michler, Micromechanical Processes and Failure Phenomena in Reactively Compatibilized Blends of Polyamide 6 and Styrenic Polymers. II. Polyamide 6/Styrene-acrylonitrile Copolymer Blends, *J. Appl. Polym. Sci.* **2010**, *115*, 2529–2539.
[34] W. Zhang, X. Guo, G. S. Kassab, A Generalized Maxwell Model for Creep Behavior of Artery Opening Angle, *J. Biomech. Eng.* **2008**, *130*, 054502.
[35] B. Bhushan, R. Jayantha-Rao, Modeling of Creep and Shrinkage Behavior of Polymeric Films Used in Magnetic Tapes, *J. Appl. Polym. Sci.* **2004**, *91*, 78 – 88.
[36] X. Liu, S. Zhang, X. Xu, Z. Zhang, L. Zhou, G. Zhang, Study on the Creep and Recovery Behaviors of UHMWPE/CNTs Composite Fiber, *Fibers Polymers* **2013**, *14*, 1635 – 1640.

Received: August 26, 2014
Published online: November 17, 2014

